Experimental and Numerical Investigations of Annular Freejets

KOBAYASHI, Hideyuki; NAKAGAWA, Tadashi; NISHIDA, Michio

Experimental and Numerical Investigations of Annular Freejets

By

Hideyuki KOBAYASHI,* Tadashi NAKAGAWA* and Michio NISHIDA*

(Received December 24, 1984)

Abstract

The structure of an axisymmetric freejet issuing from an annular orifice is described for the stagnation chamber to ambient pressure ratio of 13. The flowfield is numerically calculated. In the calculations, the physical plane is transformed to the computational one because of taking more grid points in the vicinity of the orifice. For two-dimensional calculations, the operator splitting method is used, and also the two-step Lax-Wendroff scheme is applied to each operator. To verify the computational data, laser interferometry is employed to determine the density in the freejet. The radially resolved densities are determined by means of the Abel inversion. The experimental results show a fairly good agreement with the computational results.

1. Introduction

When rocket exhaust-nozzles operate at extremely high altitudes, the chamber to ambient pressure ratio will be increased. In such conditions, the flowfield within the annular exhaust jet is very complicated to be analyzed, so that for the purpose of obtaining a fundamental knowledge of the annular-jet structure, it is desirable to investigate more simple sets such as freejets issuing from an annular orifice. According to Sule and Mueller,[1] who investigated an annular truncated plug nozzle flowfield, for large values of the chamber to ambient pressure ratio, the near wake behind the base of the plug nozzle is closed and the jet boundary is expanded beyond the outer diameter of the annular nozzle. The feature of this flowfield will be very similar to that realized by the annular freejet under consideration. The present annular freejet is such that the gas freely expands through an annular orifice from a stagnation chamber into a vacuum chamber, and it has a stagnation chamber pressure of an order of 100 torr. Therefore, this freejet may be considered as weakly rarefied. Furthermore, the chamber to ambient pressure ratio of 13 is considered.

* Department of Aeronautical Engineering

This value falls within the closed wake regime explained by Sule and Mueller.

The present work is concerned with measurements of axial and radial variations of the density in the annular freejet by means of laser interferometry, and a comparison of these with the numerically calculated results. In a previous paper,[2] the authors applied laser interferometry to the density measurements in the freejet issuing from a circular orifice, and concluded that laser interferometry is suitable to the density measurements of weakly rarefied gas flows. The experimental part of the present investigations is an extension of the previous work[2] to such a more complicated flowfield as an annular freejet. The calculations are carried out based on the operator splitting method, and the two-step Lax-Wendroff scheme is applied to each operator.

2. Numerical Analysis

2. 1 Governing Equations and Boundary Conditions

The present flow is such that, as shown in Fig. 1, the gas expands from an annular orifice into a vacuum chamber as freejet. We assume that the flow at the orifice is uniform and parallel to the freejet axis with a Mach number of unity. This freejet is treated as inviscid, compressible and axisymmetric. The variables are normalized with respect to the the stagnation state and the inner diameter of the annular orifice as follows:

$$\bar{\rho} = \rho/\rho_0,\ \bar{u} = u/a_0,\ v = \bar{v}/a_0,\ \bar{e} = e/\rho_0 a_0^2,$$
$$\bar{p} = p/p_0,\ \bar{z} = z/D_i,\ \bar{r} = r/D_i,\ \bar{t} = a_0 t/D_i,$$

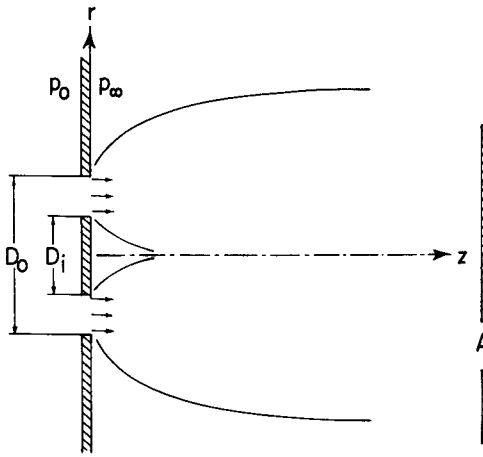

Fig. 1 A Freejet Issuing from an Annular-Orifice.

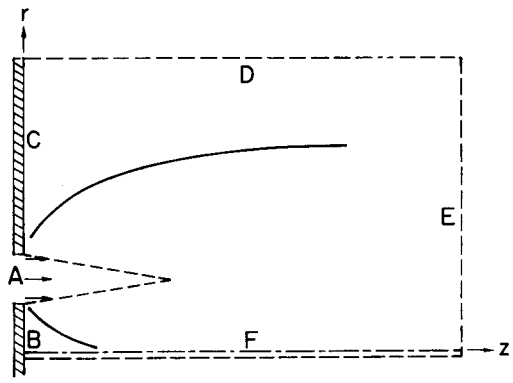

Fig. 2 Boundaries in the Computational Domain.

where ρ is the density, u is the axial velocity, v is the radial velocity, e is the total

energy expressed by $\rho[c_vT + (u^2+v^2)/2]$, where c_v is the specific heat at constant volume, p is the pressure, a is the speed of sound, t is the time, z is the axial coordinate, r is the radial coordinate, D_i is the inner diameter of the annular orifice and the subscript o denotes the stagnation condition. The governing equations for an unsteady, axisymmetric inviscid flow are written in the form

$$\frac{\partial U}{\partial \bar{t}}+\frac{\partial F}{\partial \bar{z}}+\frac{\partial G}{\partial \bar{r}}+Z=0 \tag{1}$$

with $$U=\begin{bmatrix}\bar{\rho}\\ \bar{\rho}\,\bar{u}\\ \bar{\rho}\,\bar{v}\\ \bar{e}\end{bmatrix}, \qquad F=\begin{bmatrix}\bar{\rho}\,\bar{u}\\ \bar{\rho}\,\bar{u}^2+\bar{p}/\gamma\\ \bar{\rho}\,\bar{u}\,\bar{v}\\ \bar{u}(\bar{e}+\bar{p}/\gamma)\end{bmatrix},$$

$$G=\begin{bmatrix}\bar{\rho}\,\bar{v}\\ \bar{\rho}\,\bar{u}\,\bar{v}\\ \bar{\rho}\,\bar{v}^2+\bar{p}/\gamma\\ \bar{v}\,(\bar{e}+\bar{p}/\gamma)\end{bmatrix}, \qquad z=\frac{1}{\bar{r}}\begin{bmatrix}\bar{\rho}\,\bar{v}\\ \bar{\rho}\,\bar{u}\,\bar{v}\\ \bar{\rho}\,\bar{v}^2\\ \bar{v}\,(\bar{e}+\bar{p}/\gamma)\end{bmatrix},$$

where γ is the ratio of the specific heats.

The governing equations are numerically solved by means of the finite difference method. The steady state solution is obtained as the asymptotic solution to the unsteady equations, with steady flow boundary conditions, for large time. The initial conditions are arbitrary and the steady state solutions are independent of the initial conditions. The initial conditions used here are as follows (cf. Fig. 2) : the conditions within the triangle are given by the sonic conditions; the conditions outside of the triangle are given by the ambient conditions.

The steady state boundary conditions are taken as follows: the upstream conditions at orifice A are given by the sonic conditions; the boundary conditions at wall B arise with reflection; the boundary conditions C and D are taken from the ambient conditions; the downstream conditions at E are determined by the outflow conditions ; across the centerline F, the symmetry conditions are employed.

2. 2 Coordinate Transformation

In the vicinity of the orifice, it is desirable to raise a spatial resolution for the calculations. For this purpose, $\bar{z}$ and $\bar{r}$ are transformed to P and Q, respectively, with the transformations $\bar{z} = f(P)$ and $\bar{r} = g(Q)$. Furthermore, the dependent variables U, F, G and Z are also transformed to U^*, F^*, G^* and Z^*, respectively, as follows:

$$U^* = JU\,,\quad F^* = \bar{r}_Q F\,,\quad G^* = \bar{z}_P G\,,\quad Z^* = JZ\,,$$

with $\quad \bar{z}_P = d\bar{z}/dP\,,\ \bar{r}_Q = d\bar{r}/dQ\,,\ J = \bar{z}_P \bar{r}_Q$

With these transformations, Eq. (1) is rewritten in the form

$$\frac{\partial U^*}{\partial \bar{t}} + \frac{\partial F^*}{\partial P} + \frac{\partial G^*}{\partial Q} + Z^* = 0\,.$$

In the present work, the transformations from the physical plane $(\bar{x},\bar{r})$ to the computational plane (P,Q) are made based on the following relations:

$$\bar{z} = P + a_1[\exp\,(-a_2 P)\,-1]\,,$$

$$\bar{r} = Q + b_1\{\tanh\,(-b_2 Q_0)\,-\tanh[b_2\,(Q-Q_0)\,]\} + \bar{r}_0\,,$$

with $\quad Q_0 = c - b_1 \tanh\,(-b_2 c)\,,$

where a_1, a_2, b_1, b_2, c and $\bar{r}_0$ are the constants, and these are to be determined in such a way that $\bar{x}$ and $\bar{r}$ satisfy the following requirements: 1) $\bar{z}=0$ when $P=0$; 2) four grid points are able to be taken at the orifice plane; 3) $\bar{r}(-\Delta) = \bar{r}(\Delta)$, where Δ is a half of the spatial increment. In the present computations, we take the following values for these constants: $a_1=1$, $a_2=0.5$, $b_1=0.815$, $b_2=0.655$, $c=1.18$ and $\bar{r}_0 = -9.83 \times 10^{-4}$. The computational domain used in the present work is

$$0 \le P \le P_{\max}\,,\quad -\Delta \le Q \le Q_{\max}\,,$$

where $\quad P_{\max}=9.5,\ Q_{\max}=4.5,\ \Delta=0.05,\ \Delta P=\Delta Q=0.1.$

2. 3 Numerical Method

The numerical solutions of the governing equations are based on the operator splitting method for the finite difference scheme. Let L_k^x and L_k^y be difference operators of the second-order accuracy in space for x- and y-axes, respectively. Then we have at time step $N+1$

$$U^{N+1} = L_{k/2}^x\, L_k^y\, L_{k/2}^x\, U^N\,,$$

where k is the time increment; The two-step Lax-Wendroff scheme is applied to the

operators L_k^x and L_k^r. The size of the time increment has been determined from the CFL criterion.

2. 4 Numerical Results

The numerical calculations were carried out with the following conditions: 1) the gas is a diatomic gas; 2) the outer and inner diameters of the annular orifice are $\bar{r}_o = 0.7$ and $\bar{r}_i = 0.5$, respectively. These conditions are based on the experimental conditions described later. The steady state solutions were obtained after the time steps of 1400.

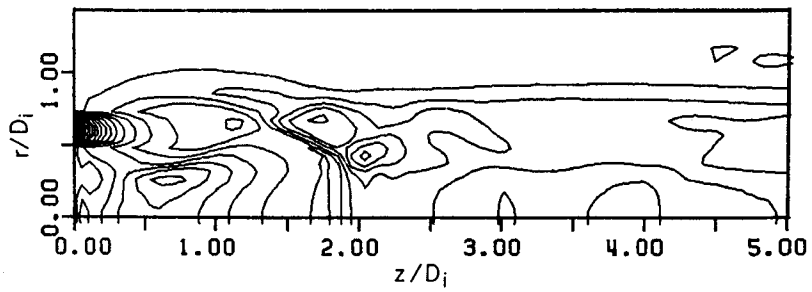

Fig. 3 Density Contours.

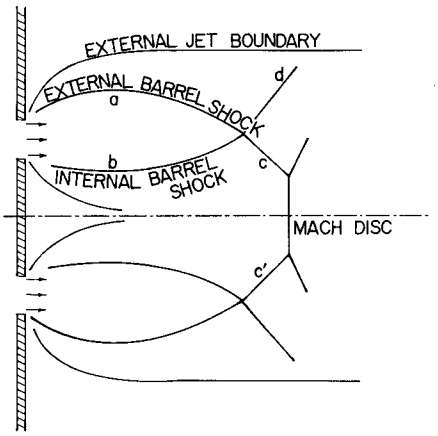

Fig. 4 Flowfield of the Annular Freejet.

In Fig. 3 is shown the density contours which were constructed by using the numerical data. The flow issues from the annular orifice which is located between $\bar{r}$ =0.5 and 0.7 at $\bar{z}$=0, and it is to the right. Based on this figure, we made a sketch

shown in Fig. 4. The shocks (a and b in the figure) are developed from the orifice. They correspond to a barrel shock which is observed in a freejet issuing from a circular orifice. These shocks meet at a point, and then two reflected shocks (c and d) are generated. The inner reflected shock (c) and another inner reflected shock (c′) construct a normal shock at $\bar{z} \simeq 2$. This normal shock may be considered as a Mach disc for the annular freejet.

According to Ashkenas and Sherman[3], the Mach disc position for a circular freejet, z_M, is given by $z_M/D = 0.67\,(p_0/p_\infty)^{1/2}$, where D is the orifice diameter, and p_0 and p_∞ are the stagnation and ambient pressures, respectively. When this relationship is applied to the present pressure ratio, $z_M/D_0 = 2.40$ is obtained, where the outer diameter of the annular orifice, D_0, should be taken in using the relation for the prediction of the Mach disc position. The Mach disc position calculated for the present annular freejet, z_M/D_i, corresponds to $z_M/D_0 = 1.43$. This is smaller than the Mach disc position for the circular freejet. The Mach disc position for the annular freejet will be increased with a decrease in the inner diameter of the annular orifice, and then reach $z_M/D_0 = 2.40$ when the inner diameter vanishes.

3. Experiment

3. 1 Experimental Apparatus and Procedure

For the purpose of experimentally verifying the numerical data, density measurements in the annular freejet were made by means of laser interferometry. The measurements were carried out in a low-density wind tunnel with nitrogen as a test gas. The experimental apparatus used here is schematically shown in Fig. 5 The test gas expands through an annular orifice into a vacuum chamber (2700 liters) as an axisymmetric annular freejet. The annular orifice has an inner diameter $D_i = 5$mm and an outer diameter $D_0 = 7$mm. The experimental conditions were such that the stagnation pressure $p_0 = 14.9$ kPa and the ambient pressure (vacuum chamber pressure) $p_\infty = 1.14$ kPa.

The arrangement of the optical system for the laser interferometry is shown in Fig. 6. The principle and data analysis of the laser interferometry is described in detail in Ref. 2, so that we do not explain these at length. After a linearly polarized laser beam from a He-Ne laser ($\lambda = 632.8$nm) is transformed to a circularly polarized beam by a quarter wave plate, it travels through the first Wollaston prism and is split into two beams with mutually perpendicular polarization directions. A lens placed at the distance of its focal length from the Wollaston prism makes the two beams parallel, which then pass through the freejet. The Wollaston prism had a splitting angle of 3.9° which generated the distance of 13.6mm between the two

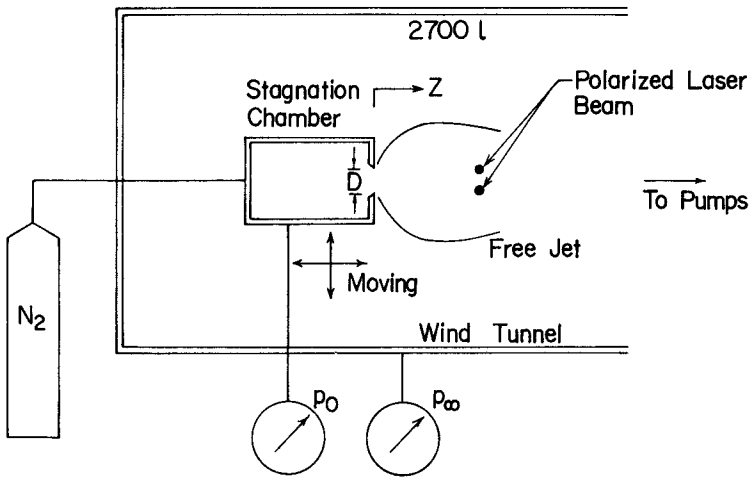

Fig. 5 Experimental Apparatus.

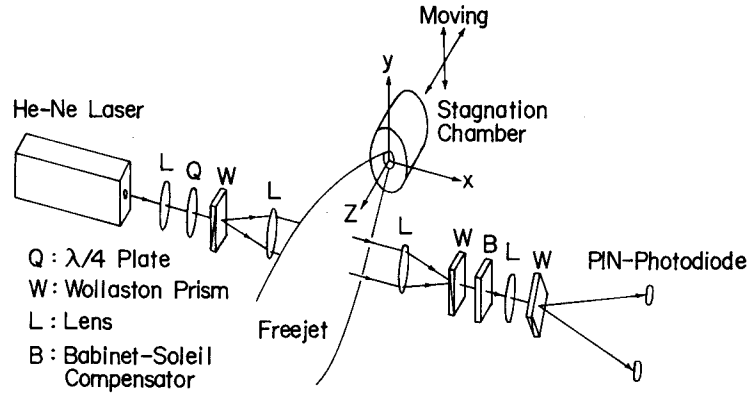

Fig. 6 Optical System for Laser Interferometry.

parallel beams in the test object, by using the lens having a focal length of 200mm. A change in the optical path occurs between the two beams due to the non-uniformity in the freejet density. After passing through the second lens and Wollaston prism, the two beams are recombined. Finally, the recombined beam is split into two interfering pairs of beams. The intensities of these two beams detected by two separate PIN silicon photodiodes (HAMAMATSU TV S-1190-01) .
A change in the difference between the output voltages from the two photodiodes, ΔU, corresponding to the change in the density difference between the two laser beams in the freejet, $\Delta\rho$, can be given by

$$\frac{\Delta U}{U_0} = \frac{\pi K}{\lambda \rho_s} \int_0^L \Delta\rho \, dx$$

where U_0 is the amplitude for the optical interference curve, ρ_s is the density at the standard state, K is the non-dimensional Gladstone-Dale constant for the standard state, L is the width of the test object and x is taken in the direction of the beam propagation.

The stagnation chamber is vertically traversed so that radial survey of ΔU is able to be made. From this survey, the radial distribution of $\Delta\rho$ is determined by means of the Abel inversion. This is done as follows: in the present work, $\Delta\rho$ is expressed as a polynomial of r (freejet radius) of even powers and the coefficients of the terms on the polynomial are determined from the radial data of ΔU.[2] If the ambient density is taken as reference density, we can easily determine the radial distribution of the freejet density by adding $\Delta\rho$ to the ambient density. The radial data of ΔU were taken at intervals of 1 mm from a location 2mm downstream from the orifice.

3. 2 Experimental Result and Comparison with Numerical Data

In Fig. 7 is shown the measured axial profile of density along the axis issuing from the middle point ($r/D_i=0.6$) between the outer and inner edges of the annular orifice. The comparison between the experiment and calculation is also depicted in the figure. The calculated result agrees fairly well with the experimental one. According to both results, the freejet density rapidly decreases from $\rho/\rho_0=0.63$ at the orifice to $\rho/\rho_0=0.03$ at $z/D_i=1.1$, and then increases. This increase is caused by compression due to the inner barrel shock shown c in Fig. 4. Behind this barrel shock, the density profile shows a small decrease and then only a weak variation. The minimum density $\rho/\rho_0=0.03$ at $z/D_i=1.1$ corresponds to a Mach number of 2.9 if the flow from the orifice to $z/D_i=1.1$ is assumed to be isentropic.

Fig. 8 shows the on-axis profiles of the experimental and numerical densities. The results show that, apart from a small peak in the vicinity of the orifice, the profiles show two peaks in the density, not only in the numerical result but also in the experimental result. However, the numerical peak precedes the experimental one. An increase in the density can be observed at $z/D_i=2$. This is caused by the Mach disc shown in Fig. 5. Upstream from the Mach disc, the density increases to $\rho/\rho_0=0.18$, and then decreases. Although this variation can be observed in both the calculated and experimental results, the agreement of both results is poor. Immediately behind the Mach disc, the experimental peak density falls over the calculated one. Downstream from the Mach disc, the experimental density decreases more

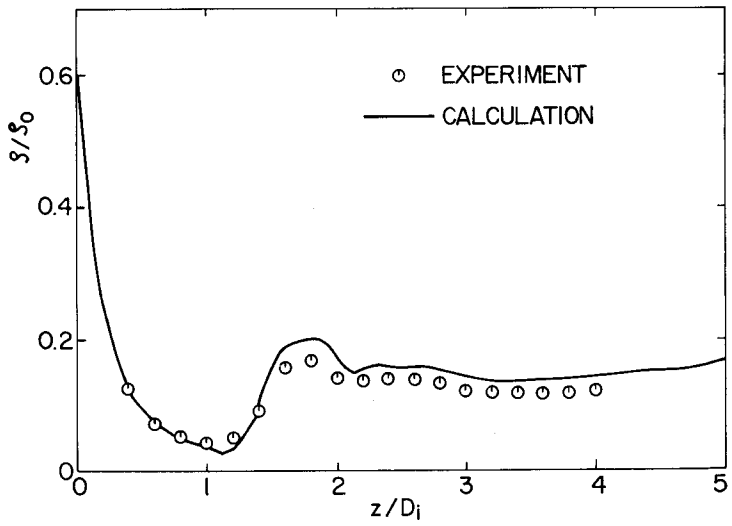

Fig. 7 Profiles of Experimental and Calculated Densities along the Axis Issuing from the Middle Point between the Outer and Inner Edges of the Annular Orifice.

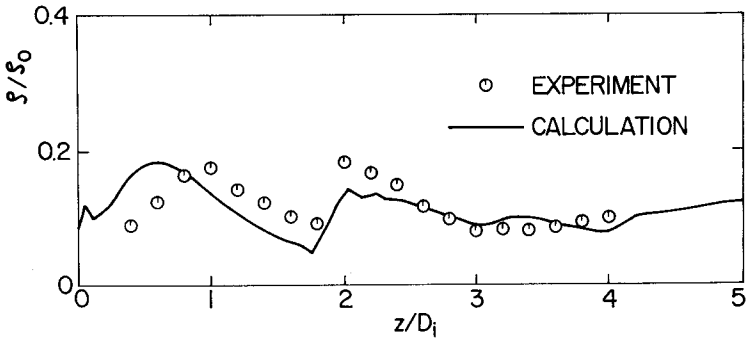

Fig. 8 On-Axis Profiles of Experimental and Numerical Densities.

rapidly than the calculated one. This decrease is due to reacceleration.

4. Conclusion

In the present work, the freejet issuing from the annular orifice, having an outer and inner diameter ratio of 1.4, has been numerically and experimentally investigated, and the following conclusions may be drawn:

(1) The density contours made, based on the numerical data, show that the annular freejet has both outer and inner barrel shocks, their reflected shocks and a

Mach disc. The existence of the Mach disc has been verified by the present experiment though the position of the numerical Mach disc slightly precedes the experimental one.

(2) Behind the Mach disc, the flow reacceleration and weak compression are repeated. However, in this region, the variation in density is comparatively small.

References

1) W. P. Sule and T. J. Mueller, J. Spacecraft **10**, 689 (1973).
2) H. Kobayashi, T. Nakagawa and M. Nishida, Trans. Japan Soc. Aero. Space Sci. **27**, 184 (1984).
3) H. Ashkenas and F. S. Sherman, Rarefied Gas Dynamics (Ed. J. H. deLeeuw) Academic Press, New York, 84 (1966).